ELSEVIER

Contents lists available at ScienceDirect

Journal of Power Sources

journal homepage: www.elsevier.com/locate/jpowsour





A computational workflow for the simulation of solid state battery electrodes from manufacturing to electrochemical performance

Siwar Ben Hadj Ali ^{a,b,c}, Mohammed Alabdali ^{a,b}, Virginie Viallet ^{a,b}, Vincent Seznec ^{a,b,c}, Alejandro A. Franco ^{a,b,c,d,*}

- ^a Laboratoire de Réactivité et Chimie des Solides (LRCS), Université de Picardie Jules Verne, Hub de l'Energie, UMR CNRS 7314, 15 Rue Baudelocque, 80039, Amiens, France
- b Réseau sur le Stockage Electrochimique de l'Energie (RS2E), Hub de l'Energie, FR CNRS 3459, 15 Rue Baudelocque, 80039, Amiens, France
- ^c ALISTORE-European Research Institute, Hub de l'Energie, FR CNRS 3104, 15 Rue Baudelocque, 80039, Amiens, France
- ^d Institut Universitaire de France, 103 Boulevard Saint Michel, Paris, 75005, France

HIGHLIGHTS:

- FEM model for ASSB cathodes to evaluate performance based on manufacturing.
- First of its kind to model the electrochemical behavior of electrodes manufactured by wet processing.
- Reduced activation overpotential and ionic resistance with conventional calendering.
- Calendering minimizes ionic flux bottlenecks and ionic concentrations gradients.
- Need for optimized manufacturing techniques to meet industrial requirements.

ABSTRACT

All-solid-state lithium ion batteries (ASSBs) have the potential to deliver higher energy and power densities compared to conventional lithium-ion batteries with liquid electrolytes. Due to the use of solid electrolytes, a uniform distribution and close contact between the active material (AM) and solid electrolyte (SE) particles are essential for a proper electrochemical behavior of the electrodes. Thus, understanding the correlation between the microstructure of composite electrodes, charge transport, and cell performance is critical. The composite cathode microstructure composed of Li₆PS₅Cl and NCM622 obtained from the simulation of its wet manufacturing process is used to implement a 4D (3 spatial coordinates, and time) computational model that simulates the electrochemical behavior during an ASSB cell discharge. The study explores the effect of the conventional calendering technique during manufacturing, demonstrating that the spatial distribution of phases and the presence of residual voids significantly influence percolation, impacting ionic and electronic conduction as well as the electrochemically active surface area. Consequently, these factors dictate the overall performance of the ASSB cell. Our findings highlight the importance of a homogeneous, compact cathode microstructure for achieving optimal ion and electron transport, ultimately enhancing the performance of ASSB cells.

1. Introduction

Lithium-ion batteries (LIBs) play a pivotal role in various applications, including stationary energy storage systems and electric or hybrid vehicles. However, conventional LIBs are approaching their physical limits in terms of energy density and fast-charging capabilities [1,2]. In this context, all solid-state lithium ion batteries (ASSBs) represent a promising alternative, offering the potential for significantly higher power and energy density while also addressing critical safety concerns. Despite their promise, ASSBs present numerous challenges that are the

focus of ongoing research.

The solid-state nature of all ASSB cell components, combined with the volume changes of the active materials during (de-)lithiation, introduces complex interplays between electrochemical, transport and mechanical processes, which strongly affect the overall cell performance [3–5]. In LIBs, electrodes are typically designed as porous microstructures that allow the liquid electrolyte to infiltrate, ensuring significant wetting of the active material (AM) across all regions and enabling relatively short pathways for ion transport [6,7]. However, the scenario changes in ASSBs as the inorganic solid electrolyte (SE) is already

E-mail address: alejandro.franco@u-picardie.fr (A.A. Franco).

https://doi.org/10.1016/j.jpowsour.2024.236131

^{*} Corresponding author. author. Laboratoire de Réactivité et Chimie des Solides (LRCS), Université de Picardie Jules Verne, Hub de l'Energie, UMR CNRS 7314, 15 Rue Baudelocque, 80039, Amiens, France.

integrated into the electrode during fabrication. As a result, achieving a uniform distribution and full contact between AM and SE particles is not easy to achieve [8], leading to more complex microstructural challenges than in traditional LIBs.

In ASSBs, the SE, alongside the AMs, plays a critical role by providing chemical stability and an ionic conductivity exceeding several mS.cm⁻¹ at room temperature, which is necessary to match the performance of conventional LIBs. Among a multitude of material classes of solid electrolytes, lithium thiophosphates demonstrate the highest conductivities, some of which exceed 20 mS.cm⁻¹ [9,10]. Beyond their high conductivity, thiophosphate-based SEs stand out also due to their unique mechanical properties, especially their malleability caused by low Young's moduli, which allows the electrodes to be densified at low temperatures without the need for energy-intensive sintering processes [11,12].

A number of research groups have investigated the microstructure of ASSB electrodes through modeling and charge transport measurements [13-21]. These studies have demonstrated a direct correlation between the microstructure architecture and the percolating behavior of SE, which also impacts the active surface area available for Li-ion insertion. Therefore, the performance of ASSBs is significantly influenced by factors such as material composition [14,15], microstructural arrangement [17,21], particle size [16–20], and manufacturing conditions [13]. Among these studies, several of them have directly linked charge transport measurements of ASSB cathodes with detailed microstructural information obtained from tomography [18] or from manufacturing process simulation by our group [13]. For instance, Minnmann et al. [8] identified SE particle size as a critical parameter determining charge transport in 3D-reconstructed composite cathode microstructures obtained by Focused Ion Beam-Scanning Electron Microscopy (FIB-SEM), accounting for tortuosity effects and structural inhomogeneities. Alabdali et al. from our group [13] simulated in 3D a slurry-based manufacturing process (wet processing) of ASSB composite cathodes, incorporating conventional manufacturing parameters, and demonstrated that the degree of compression applied during the cathode manufacturing significantly affects the ionic and the electronic charge transport in thiophosphate-based electrodes. Other studies have also linked in 3D the electrode performance with its composite microstructure. For example, Neumann et al. [18] combined theoretical and experimental approaches to identify the limiting factors for the electrochemical performance of β-LPS-based ASSBs using microcomputed tomography (micro-CT) images. The findings were that a reduced contact between the electrode layer and the current collector, along with delamination of the SE from the active particle surface, significantly influences cell performance. Another noteworthy study by Bielefeld et al. [17] examined the influence of lithium-ion kinetics, particle arrangement, and void distribution on the electrochemical performance of NMC622/Li₆PS₅Cl composite cathodes, employing stochastically generated cathode microstructures. Their study resulted in a proposed optimized microstructure aimed at improving performance. Nonetheless, key limitations of their study include the stochastic nature of the microstructure generation process and the absence of carbon and binder domains. While a stochastic microstructure generation does not allow to investigate the influence of manufacturing parameters, the lack of the consideration of carbon and binder does not allow to reflect real-world cathodes.

Here, we present, for the first time to our knowledge, a comprehensive computational modeling workflow that examines the influence of the degree of calendering on the final performance of slurry-based composite electrodes. This study uses NMC622/Li₆PS₅Cl-based cathode microstructures with the presence of carbon and binder, generated through conventional calendering, via manufacturing process simulations. This computational workflow is able to correlate the manufacturing process, the composite cathode microstructure and the cell performance, as it combines Coarse-Grained Molecular Dynamics (CGMD) for the manufacturing simulation of the slurry, drying and calendering with a 4D-resolved performance model describing

electrochemistry and transport mechanisms. The three-dimensional spatial locations of AM, SE, and Carbon-Binder Domain (CBD) within the electrode, as predicted from CGMD simulations, are considered explicitly as separated phases, each of them with specific physical properties. Our computational modeling workflow, allowing to perform simulations from the solvent-based manufacturing process to the electrochemical performance of the resulting ASSB cathodes, permits the study of the impact of the calendering on ionic flux bottlenecks, the heterogeneities of electrochemical reactivity within the electrode volume, and the resulting overall electrochemical performance. These features make our modeling approach a powerful tool to provide guidance for optimized manufacturing of the ASSB cathodes with wet-processing methods.

2. Model description

Our computational modeling workflow consists of two main parts. The first part is already published [13] and devoted to the generation of the electrode microstructures under different degrees of calendering using the CGMD modeling technique. The second part is devoted to the simulation of the electrochemical behavior of the electrodes upon discharge by using the Finite Element Method (FEM).

2.1. Electrode microstructure generation

The manufacturing process of the NMC622-based electrodes was performed experimentally and reported by Alabdali et al. [13]. By using the obtained manufacturing properties, a predictive model was carried out by simulating in 3D a slurry-based manufacturing process of ASSBs composite electrodes using the CGMD technique in LAMMPS [22] computational software. It involves three major steps in the electrode wet manufacturing process: the slurry preparation, the drying and the calendering as shown in Fig. 1. These simulations account for the AM, the SE and the CBD but it does not distinguish explicitly between carbon and binder. The CGMD technique is based on applying force fields/contact forces representing the interaction between particles and their mechanical properties, and these force fields were parameterized to match experimental properties.

From the slurry to the dried electrode, the CBD particles containing solvent shrunk to the diameter corresponding to the solid size to mimic the evaporation of the solvent, and the calendering step was modeled by a plane moving downward at constant speed to compress the electrode while maintaining the bottom surface fixed. The readers can refer to our previous work for more details about the simulation of the slurry, drying and calendering process [23–25].

Different microstructures were generated from our CGMD model as illustrated in Fig. 2a, each one corresponding to a different calendering degree, i.e. a different percentage of reduction of the thickness due to the applied calendering pressure. The usability of this model is limited for calendering degrees under or equal to 35 %, as it was discussed in Ref. [13] because above 35 % a decrease in the electrical conductivity was observed due to the partial occupation of the volume of CBD particles by other materials due to high pressure. For the following, we will work with the microstructures presenting three different compression degrees (0 %, 20 %, 35 %), each one corresponding to different volume fractions of AM, SE and CBD, different thickness and different porosity as displayed in Table S1. Thus, the effect of microstructural variability on the effective electrode properties (i.e. ionic tortuosity, active area and effective conductivities) is considered in this work. Readers can refer to our previous publication [13] for a detailed understanding of the microstructural characteristics evolution with varying degrees of calendering.

2.2. Microstructure post-processing

The transformation from spherical to irregular particle shapes in our

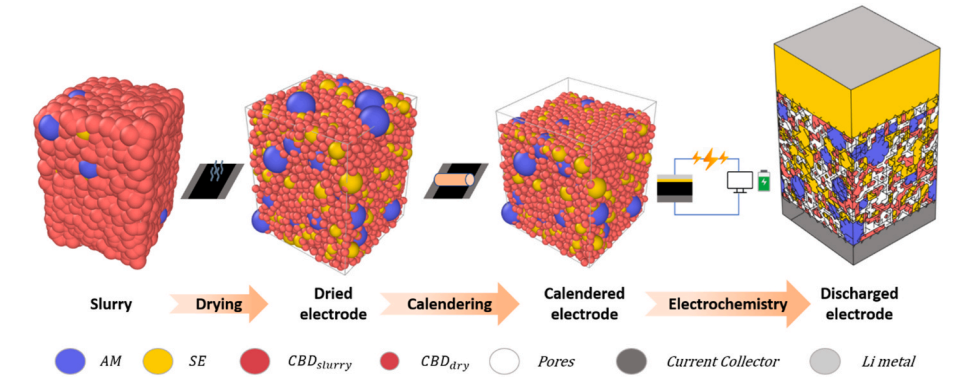


Fig. 1. Schematic of our computational workflow simulating the wet manufacturing process of ASSB composite cathodes: from slurry to calendered electrode followed by the half-cell electrochemical performance simulation. Adapted with permission from Alabdali et al. [13].

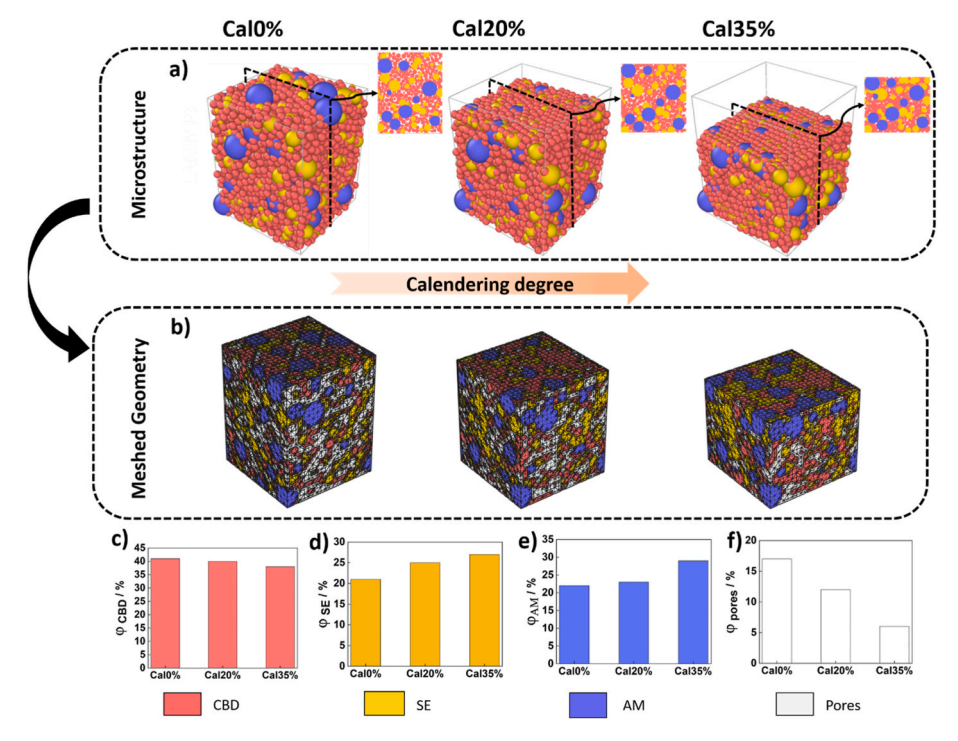


Fig. 2. (a) Composite electrode microstructures for the 10 %, 20 % and 35 % calendering degrees obtained from the manufacturing simulation developed using the CGMD technique, (b) Composite electrode microstructures after the multi-phase meshing process using our INNOV software and (c, d, e, f) volume fractions of AM, SE, CBD and pores for each calendering degree, respectively.

FEM electrochemical modeling environment is a result of a specific postprocessing step performed on the CGMD simulation data. During this step, overlaps are handled based on the prioritization of the AM then the SE and finally the CBD. For each instance of overlap between AM and CBD or between AM and SE, we adjust the volume calculations by reducing the volume attributed to the CBD and adding this reduced volume to the AM or SE, respectively. This adjustment implicitly considers the porosity of the CBD by reducing its presence in overlapping regions, as one knows that CBD can be porous [26]. Moreover, it reflects the spatial redistribution of material, leading to the transformation of the initially spherical particles into more realistic, irregular shapes for AM, SE and CBD. This approach has been used in our group previously for LIB electrodes simulation [24]. It ensures a more realistic representation of the microstructures, capturing the inherent irregularities and complexities observed in the actual materials, thus enhancing the fidelity of the electrochemical model.

The use of a meshing technique constitutes the second step for the importation of the electrode microstructures generated from the CGMD

modeling workflow into our 4D-resolved electrochemistry simulator. The meshes have been generated with our *in house* software INNOV [27, 28], which relies on a voxelization technique to create multi-phase volumetric meshes for FEM calculations. Meshed electrode microstructures for 0 %, 20 % and 35 % calendering degrees, which are referred to hereafter as Cal0%, Cal20% and Cal35%, are provided in Fig. 2b.

2.3. Electrochemical model

We use our 3D-resolved performance model with a Li-foil for the anode, $\rm Li_6PS_5Cl$ for the separator and for the composite electrode generated by our manufacturing simulations, to evaluate how the differences in the calendering degree impact the electrochemical response (cf. Fig. 1). The electrochemical evaluation of the ASSB cell is conducted without the application of any external forces, with the calendering process applied exclusively before the electrochemical simulation. This approach allows us to isolate and analyze the intrinsic effects of calendering on the cell performance. The commercial software COMSOL

Multiphysics® [29] was used as our FEM calculation platform. All the calculations were performed in the MatriCS platform (Université de Picardie Jules Verne) [30] using one node with 500 GB of RAM and 1 processor (Intel® Xeon® CPU E5-2680 v4 @ 2.40 GHz, 28 cores). The computational domain of our electrochemical model consists of four phases: AM, CBD, SE and current collector CC.

The first material domain is the AM which features ionic and electronic transport. The lithium transport within the AM particles has been solved using Fickian diffusion as given below

$$\frac{\partial C_s}{\partial t} = -\nabla(-D_{AM}\nabla C_s) \tag{1}$$

where C_s is the lithium concentration in AM particles, D_{AM} , the lithium diffusion coefficient inside the AM (dependent on the state of charge (SOC) and derived from the experimental data reported by Bielfeld et al. [31]) and t is time. The electric potential (ϕ_s) in each of the AM, CBD and CC domains can be solved by using Ohm's law as follows

$$\nabla (-\delta_{e,i} \nabla \phi_s) = 0 \tag{2}$$

Here, $\delta_{e,i}$ is the effective electronic conductivity of the domain, where i represents AM,CBD or CC. Moreover, the electric potential (ϕ_{SE}) for ionic transport in the SE domain can be estimated using charge conservation as shown below,

$$\nabla(-\delta_{ion}\nabla\phi_{SE}) = 0 \tag{3}$$

where, δ_{ion} is the effective ionic conductivity in the SE phase. In order to capture the single ion conductor characteristics of Li₆PS₅Cl, the transference number of lithium ions is set to $t^{\rm Li+}=1$. This results in negligible lithium ion concentration gradients in the SE compared to cases with multiple mobile ionic species. Butler–Volmer kinetics is used to describe the electrochemical reaction occurring at the active AM-SE contact and is expressed as follows

$$J_{BV} = i_0 \left[exp \left(\frac{F}{2RT} \eta \right) - exp \left(\frac{-F}{2RT} \eta \right) \right]$$
 (4)

where i_0 , the exchange current density at the AM-SE interface, is dependent on the SOC and was taken from Ref. [17]. This parameter is obtained via the charge transfer resistance R_{CT} , which was measured by Electrochemical Impedance Spectroscopy (EIS) on similar interfaces [31]. This charge transfer resistance contains the exchange current density

$$R_{CT} = \frac{RT}{zFAi_0} \tag{5}$$

where, F is the Faraday constant, R is the universal gas constant, T is the temperature, A is the active surface area, z is the charge number of Li^+ (1). In. Eq. (4) η is the overpotential.

The overpotential η is given by the following expression:

$$\eta = \phi_{AM} - \phi_{SE} - V_0^{NMC622} \tag{6}$$

Here, $V_0^{\rm NMC622}$, the equilibrium potential difference in NMC622, was adapted from data in Ref. [31] for a NMC half-cell discharged at a C/10 rate in the first cycle. On the anode interface, we model the stripping of lithium metal by the Butler-Volmer equation as well. However, as this work is focused on the composite cathode, we assume a high exchange current density which is independent from the anode's SOC. The system is fully defined by a Dirichlet boundary condition on the electric potential on the anode surface ($\phi_{s,ext}=0$) and a current flux boundary condition at the free end of the CC to match the desired discharge rate. The porosity of CBD is accounted implicitly in the electrochemical model through the transport parameters of CBD. In this model and in contrast to our previous work in Ref. [32], we did not account for the volume change in AM during lithiation. As the formation of side products and the loss of contact area due to swelling and shrinking of the AM

introduces significant uncertainties in the kinetic parameters, therefore we extract AM parameters at the pristine state from previous studies. All the parameters used in the modeling framework are listed in Table S2 of the Supporting Information.

2.4. Charge transport calculations

We describe in this section the charge transport simulations carried out to correlate microstructure with transport properties. The calculations to determine the effective conductivities (δ) and geometric tortuosity (τ_g) were performed employing the ConductoDict and DiffuDict modules of GeoDict 2023 (Math2Market) [33], using a standard desktop computer. δ and τ_g are two chosen parameters to provide a quantitative indication of the effect of calendering degree on the electrode's performance. They are simple observables defined to account for both ionic and electronic properties of the simulated uncalendered and calendered electrodes. The electronic effective conductivity δ_e was calculated by solving the Poisson equation in the simulation domain, applying a 1 V potential difference between opposite sides along the z direction (perpendicular to the calendering plane). Then, Ohm's law was used to obtain the $\delta_{\text{e}}.$ The electronic conductivities of the AM and the CBD phases were set to $0.005 \text{ S} \cdot \text{m}^{-1}$ and $15.93 \text{ S} \cdot \text{m}^{-1}$ [34–36], respectively. The τ_g values were calculated from the determined effective diffusivity according to

$$\tau_{\rm g} = \sqrt{\frac{\varphi_{SE}}{D_{\rm eff}}} \tag{7}$$

where φ_{SE} is the volume fraction occupied by the SE and D_{eff} is the effective diffusion coefficient for Li ions in the SE medium. D_{eff} is in turn calculated by solving the Fick's first law in the SE domain, with a concentration difference Δc between the outer xy planes. D_{eff} is obtained from the overall diffusive flux j as

$$D_{eff} = \frac{-j \times length}{\Delta c}$$
 (8)

Since τ_g is only a geometrical magnitude, it is independent of the values chosen for Δc and the diffusion coefficient within the SE. The ionic effective conductivity δ_{ion} can be determined according to the McMullin number [37] N_M

$$N_{\rm M} = \frac{D_{\rm eff}}{D_{\rm bulk}} = \frac{\delta_{\rm ion}}{\delta_{\rm bulk}} \tag{9}$$

with D_{bulk} and δ_{bulk} stand for the bulk electrolyte diffusivity and the bulk ionic conductivity, respectively. The D_{bulk} was set at 1 m²·s⁻¹ and δ_{bulk} was provided by the supplier and it is equal to 1.25 mS·cm⁻¹. All of these input parameters were considered isotropic. Periodic boundary conditions were considered for the outer xz and yz planes.

3. Results and discussions

Simulations were performed within the voltage range of 2.6–4.2 V vs. Li $^+$ /Li for different C-rates for each degree of calendering. The key findings from the analysis of the simulated discharge curves presented in Fig. 3 are as follows. Firstly, the model accurately captures the loss of specific capacity while increasing the C-rate, *i.e.* the capacity drops from 188.28 mAh.g $^{-1}$ at C/50 to 62.8 mAh.g $^{-1}$ at C/5 for the Cal20% case. Furthermore, the specific capacity at a given C-rate is higher for the 35% calendering case than the 20% and 0% ones. This trend is similar to the one found for LIB cathodes by us [35], where we demonstrated through modeling that increased calendering reduces interfacial resistance between the CC and CBD, enhancing electronic conductivity and thus leading to better overall cell performance.

Another trend arising from Fig. 3e is the difference of specific capacity between the calendering degrees cases tends to shrink by decreasing the C-rates. At low C-rates, the difference between the three

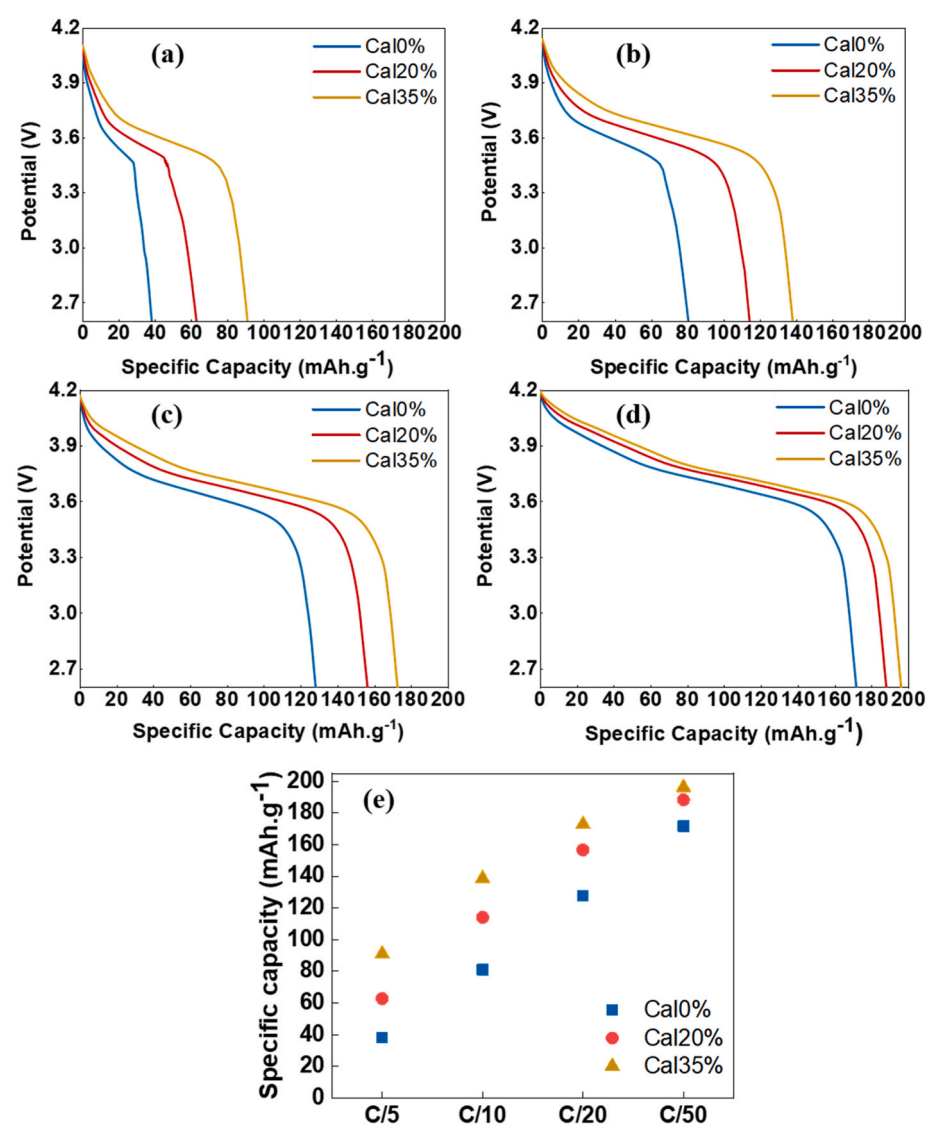


Fig. 3. Discharge curves of the composite electrodes along the Cal0%, Cal20% and Cal35% calendering degrees at (a) C/5, (b) C/10, (c) C/20, (d) C/50 and (e) Comparison of the simulated rated specific capacity of the Cal0%, Cal20% and Cal35% at the end of discharge (2.6 V).

cases is minor (Fig. 3d). However, at high C-rates, the effect is relatively prominent (Fig. 3a). This observation can be explained by the transition a kinetically-limited regime at high C-rates thermodynamically-dominated regime at lower C-rates, which is a phenomenon well known in Li ASSBs cells [38] and also, reported by our group in LIBs modeling [39]. At high C-rates, kinetic factors, such as charge transport limitations, limited active surface area and polarization effects, dominate the electrochemical behavior of the electrode. The pronounced difference in performance between calendering degrees at these rates can be attributed to variations in tortuosity factor and the accessibility of charge transport pathways. This is in line with the findings of Minnmann et al. [8], who demonstrated by modeling ASSBs electrodes corresponding to different SE particle sizes, that high C-rate performance is constrained by kinetic limitations, including increased resistance in charge transport pathways and decreased interfacial contact between AM and SE. As a result, calendering plays a significant role in eliminating these kinetic bottlenecks. On the other hand, at lower C-rates, the electrode performance is more influenced by thermodynamic factors. The relatively small difference in specific capacity across calendering degrees at low C-rates suggests that kinetic limitations are less critical under these conditions.

Fig. 4 presents the lithium concentration distributions for the

electrodes' AM at C/50 discharge rate at different cell voltages: 3.9 V, 3.65 V, and 2.6 V, corresponding to the 25 %, 75 %, and 100 % depth of discharge (DOD), respectively. Notably, the cathode with a higher degree of calendering exhibits a relatively uniform AM utilization across the entire composite cathode (Fig. 4g-i). In contrast, the uncalendared electrode in Fig. 4a-c displays localized lithiation, which is due to a reduced number of percolating pathways.

This observation is consistent with the calculated ion-flux distributions for Cal0%, Cal20%, and Cal35% at the middle of discharge, as illustrated in Fig. 5, which reveal more pronounced regions of high ionic current density. These results indicate that increased bottlenecks (*i.e.* localized regions where ion movement is significantly restricted) impede ion flow in the uncalendered electrode. These heterogeneities affect the overall efficiency of Li ion intercalation [40]. Overall, our findings clearly indicate that higher calendering degrees enhance cell performance, as they enable more homogeneous microstructure with improved percolating pathways.

To identify the underlying mechanisms behind the differences in discharge curves and microstructure, we analyzed the key electrochemical kinetics indicators that govern the system. In particular, we focused on the average reaction overpotential at the AM-SE interface and the SE potential. The observed decrease in the average reaction

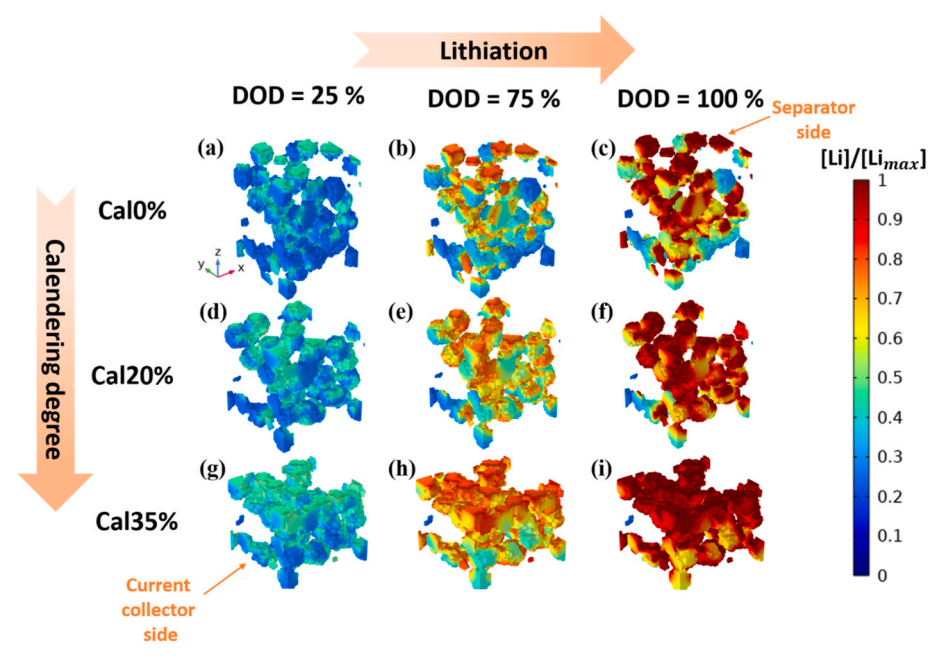


Fig. 4. Spatial distribution of the state of lithiation inside the AM phase at different depths of discharge DOD for Cal0% (a, b, c), Cal20% (d, e, f) and Cal35% (g, h, i) calendering degrees at C/50 discharge rate.

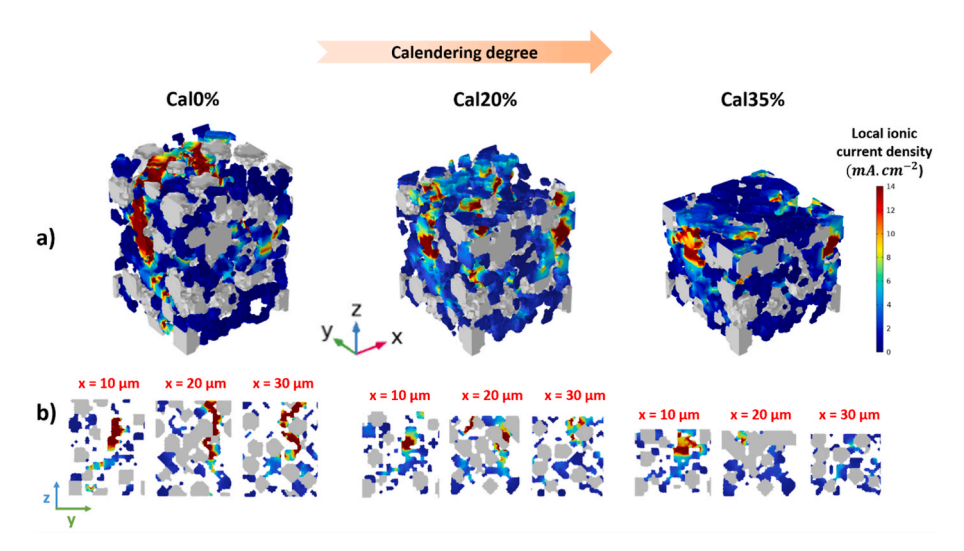


Fig. 5. a) Calcualted ionic flux-distributions at the middlle of discharge for the three composite electrodes at C/50 with different calendering degrees, b) Cross-sectional images of the electrodes with the positions as a function of x-coordinate. The uncalendered electrode exibits a localized ionic current flow more than the calendered electrodes.

overpotential (Fig. 6a) with increasing degrees of calendering can be attributed to the enhanced contact between the AM and SE particles. The high activation overpotential η_{act} for the Cal0% electrode, as shown in Fig. 6c, highlights the significant voltage loss required to drive the charge transfer process due to slow reaction kinetics at the AM-SE interface, either from a high reaction energy barrier or low reaction area [39]. Cal0% exhibits a much higher activation overpotential (η_{act}) compared to Cal20% and Cal35%, primarily due to the lower active area resulting from calendering. Fig. 6d demonstrates that the active area becomes denser and forms more continuous AM-SE contact at higher degrees of calendering. This improvement is a result of the compression applied during the calendering process, which promotes more uniform contact and reduces interfacial resistance that affects reaction kinetics. A better contact reduces energy barriers for charge transfer, allowing for more efficient electrochemical reactions at the AM-SE interface. In

parallel, the reduction in electrolyte potential with increased calendering (Fig. 6b) is largely the result of decreased ionic resistance within the SE. As calendering improves the packing density of SE particles, the ionic percolation network becomes more continuous, facilitating the movement of ions through the SE phase. This improved ionic conduction within the solid-state matrix is critical for maintaining low overpotentials during discharge and ensuring efficient operation of the cathode.

The enhanced interfacial contact and the improved ionic percolation were found to be the most significant contributors to the variations observed in the discharge profiles, their associated overpotentials, and overall electrochemical performance. A detailed investigation of these factors within the electrode microstructures, prior to cell integration, is provided in the subsequent sections.

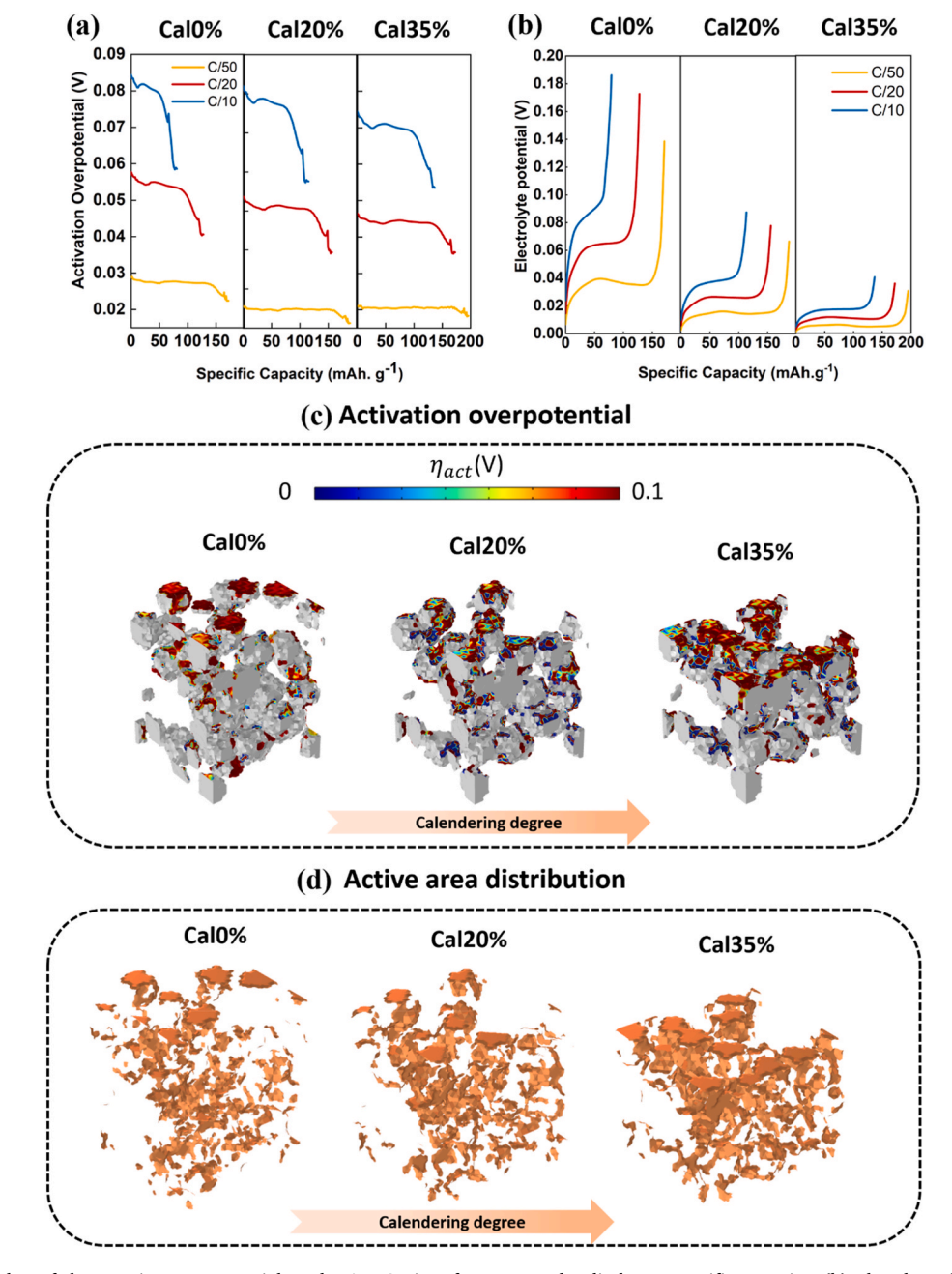


Fig. 6. (a) Average value of the reaction overpotential at the AM/SE interface versus the discharge specific capacity, (b) The electrolyte potential versus the discharge specific capacity, (c) Spatial distribution of activation overpotential η_{act} at the AM-SE reacting interface at the end of C/50 discharge for different calendering degrees, (d) The active area distribution within the composite cathode for the different calendering degrees.

3.1. Interfacial surface area

To assess how the microstructure influences the kinetics of composite electrodes, we analyzed the interface area, a key descriptor that reflects the distribution of different phases. Specifically, the interface between AM and the SE, referred to as S_{AM-SE} , is of particular importance as it is where the electrochemical reaction occurs. A large interface area is critical for minimizing charge transfer impedance [18].

As shown in Fig. 7a, the specific surface area between AM and SE increases with higher degrees of calendering, with Cal35% exhibiting the largest contact area. Consequently, the pore-coverage of the AM decreases, as $S_{AM\text{-pores}}$ reduces from 0.02 $m^2 \, g^{-1}$ for Cal0% to 0.004 $m^2 \, g^{-1}$ for Cal35%, while $S_{AM\text{-SE}}$ increases from 0.01 to 0.019 $m^2 \, g^{-1}$. This increase in AM-SE contact is attributed to the pressure applied during the calendering process, which reduces voids between the

particles as already observed in the volume fraction diagram (Fig. 2e), resulting in enhanced AM-SE connectivity. The specific surface area of the AM is measured at 0.16 m 2 ·g $^{-1}$, and the fraction of AM surface covered by SE increases from approximately 10 % at Cal0% to nearly 28 % at Cal35%. Although, for Cal35%, around 6 % of the AM surface is still in contact with pores, 24 % with CBD and 42 % with other AM particles. These findings suggest that maximizing S_{AM-SE} and minimizing residual porosity are key to fabricating highly compact electrodes, thereby optimizing the electrochemical performance of calendered electrodes. Which is in line with the findings of Bielefeld et al. [17], who demonstrated that a cone-like microstructure where the AM and the SE are arranged into conical formations in direct contact, exhibits higher values of active interface area between AM and SE compared to stochastically generated microstructures and current experimental outcomes. This enhanced active interface area contributes in a higher amount of

Ionic Conductive Network

Cal0% Cal20% Cal35% O.001 AM - pores SE - pores AM - SE

Electronic Conductive Network

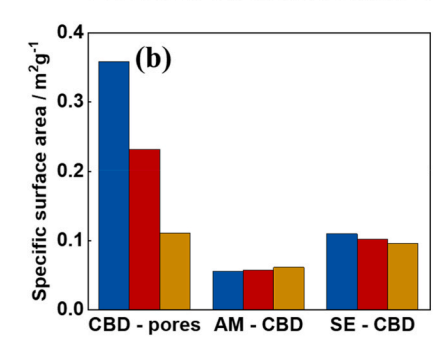


Fig. 7. Specific interface area between the different phases showing a clear dependence on the calendering degree: a) for ionic conductive network, b) for electronic conductive network.

electrochemically accessible material which determines the achievable capacity [8,16,41], thereby improving the overall performance in ASSBs.

3.2. Conductive network

In addition, we performed charge transport calculations to assess geometrical descriptors, as described in section 2.4, to further elucidate the relationship between microstructure and transport processes. The geometric tortuosity (τ_g) within the SE for the uncalendered microstructure, illustrated in Fig. 8a, was approximately 10. This high value indicates a significant degree of complexity in the ionic transport pathways, primarily due to the inhomogeneous distribution of SE particles and the limited number of continuous ionic channels. Such a microstructure presents multiple bottlenecks for ion transport, resulting in a more tortuous path for ionic conduction [15,21,42], which ultimately impairs the overall ionic mobility and, consequently, the electrochemical performance of the electrode. As the degree of calendering increases, τ_g is reduced significantly, reaching a value of around 4 in the highly calendered electrode. This marked decrease in tortuosity reflects the enhanced homogeneity of the SE particle spatial distribution [8], as well as the creation of more continuous and accessible ionic pathways. These findings are consistent with the homogenized microstructure and lithiation observed in Fig. 4, where the distribution of SE and AM particles becomes more uniform, leading to fewer localized bottlenecks in ion flux, as shown in the ion flux distribution in Fig. 5.

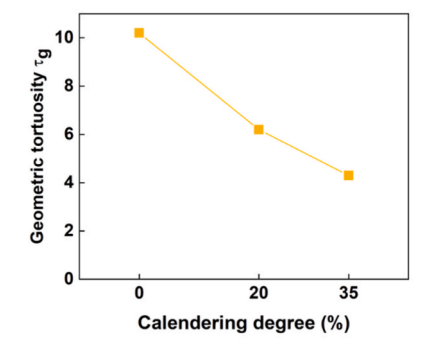
Compared to the effective ionic conductivity, the effective electronic conductivity shows less dependence on the calendering degree with $0.24~\rm mS\cdot cm^{-1}$ for the uncalendered electrode and $0.31~\rm mS\cdot cm^{-1}$ for the Cal35% electrode (Fig. 8b). The observed increase in electronic conductivity with higher calendering degrees can be directly attributed to the improved contact area between the AM and CBD, as illustrated in

Fig. 7b. This enhancement in contact area facilitates more effective electronic percolation throughout the electrode, ensuring that electrons can traverse the electrode more efficiently. The improvement in microstructural connectivity, ionic and electronic, is essential for optimizing charge transport and thereby the overall performance of the battery system. Our results clearly demonstrate that the combination of poor ionic connectivity and reduced electronic percolation leads to heterogeneous lithiation, as only certain regions of the electrode experience sufficient ionic and electronic flux for full lithiation to occur. This highlights the critical role of microstructural optimization, specifically through calendering, in achieving uniform charge distribution and maximizing electrochemical efficiency.

4. Conclusion and outlook

In this study, we introduced a 4D-resolved computational workflow that, for the first time, simulates the electrochemical performance of ASSB composite electrode microstructures obtained by manufacturing simulations. The model uses a sulfide-type SE, NMC622 as AM, and a blend of carbon and binder.

Our analysis of the electrochemical performance showed that the surface contact area is a key geometric factor in the electrode microstructure. A larger contact area between the AM and SE, resulting from the calendering process, significantly reduces ion flux bottlenecks and minimizes localized ion concentrations. We also quantified the ionic geometrical tortuosity, as well as the electrode's electronic conductivity, under different calendering conditions. These findings revealed that more compact electrode microstructures, achieved through higher degrees of calendering, shorten the pathways for charge transport, increase the number of conductive paths, and lead to more uniform lithiation throughout the cathode. The improvement of electrochemical performance with calendering is, thereby, explained by the increasing number



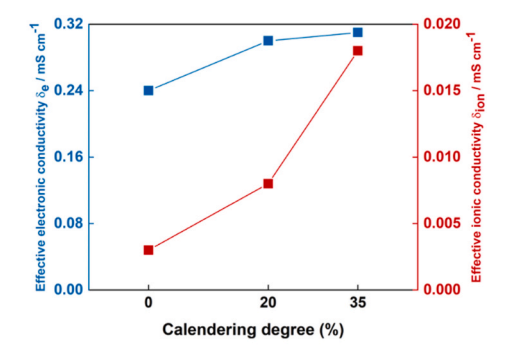


Fig. 8. Calculation results of charge transport on the reconstructed electrode microstructures corresponding to different calendaring degrees: (a) Geometric tortuosity for ionic transport, (b) Ionic and electronic effective conductivities.

of percolating pathways resulted from higher contact area between AM-SE and AM-CBD. Additionally, the heterogeneities in the state of lithiation of AM and bottlenecks of ionic current flux in the uncalendered electrode microstructure further confirm the benefits of calendering.

Overall, our results highlight that high calendering degrees are essential for optimizing the contact area between AM and SE, reducing ionic tortuosity, and improving cycling and rate performance of ASSB cells.

Despite the enhancements in overpotential and structural integrity due to calendering, the current method does not achieve the necessary C-rate performance and current density required for industrial applications, particularly under normal usage and fast charging conditions. Specifically, the capacity reaches a maximum of 200 mAh/g at a low Crate of C/50 but declines significantly at higher C-rates, far below industrial standards. This poor performance can be attributed to the conventional calendering method employed, which involves uniaxial compression. The uniaxial press method compresses the electrode material in a single dimension, resulting in suboptimal tortuosity, even at low porosity levels. Unlike traditional liquid electrolyte batteries, ASSBs do not benefit from the liquid filling the pores, which can mitigate some of the effects of high tortuosity. Therefore, while uniaxial calendering contributes to some degree of improvement, it is evident that it cannot fully meet commercial performance levels. This gap underscores the need for alternative calendering techniques (e.g. isostatic calendering) or innovative electrode fabrication methods that can further optimize the internal microstructure of ASSB electrodes, ensuring efficient ion transport and meeting the rigorous demands of industrial applications.

Future modeling work will incorporate the volume changes in AM during lithiation to capture the complex interactions between electrochemical and mechanical processes, which are crucial for the overall performance of solid-state batteries. Additionally, this research utilizes conventional unidirectional rolling calendering techniques, which might not achieve optimal internal microstructural architecture for ASSB electrodes. During the electrochemical cycling of the electrode, isostatic compression reduces the mechanical stress between the AM and SE particles in comparison to uniaxial compression, as we have reported in our previous study [32] using the Discrete Element Method (DEM) approach. Consequently, more advanced methods such as isostatic pressing rolling technology need to be considered in the future. We highlight that the current work reported in this article, aims to disclose a computational simulation workflow allowing the investigation of the effect of the calendering degree (i.e. manufacturing conditions) on the electrochemical performance of ASSB electrodes. Our future work will involve experimental studies to directly compare the simulation results with experimental data to further solidify our findings, and to explore further the interplays between electrochemistry, transport and mechanics.

CRediT authorship contribution statement

Siwar Ben Hadj Ali: Writing – original draft, Visualization, Software, Methodology, Investigation, Formal analysis, Data curation, Conceptualization. Mohammed Alabdali: Writing – review & editing, Methodology, Investigation, Formal analysis, Conceptualization. Virginie Viallet: Supervision. Vincent Seznec: Supervision. Alejandro A. Franco: Writing – review & editing, Supervision, Resources, Project administration, Methodology, Funding acquisition, Conceptualization.

Declaration of competing interest

The authors declare that they have no known competing financial interests or personal relationships that could have appeared to influence the work reported in this paper.

Acknowledgments

S.B.H.A, M.A. V.S. and A.A.F. acknowledge the support by Umicore within the DESTINY PhD Programme, which has received funding from European Union's Horizon2020 research and innovation programme under the Marie Skłodowska-Curie Actions COFUND (Grant Agreement #945357). A.A.F. and M.A. acknowledge the European Union's Horizon Europe research and innovation program under grant agreement no. 101069686 (PULSELION). A.A.F. acknowledges Institut Universitaire de France for the support.

Appendix A. Supplementary data

Supplementary data to this article can be found online at https://doi.org/10.1016/j.jpowsour.2024.236131.

Data availability

Data is available upon reasonable request.

References

- [1] K.G. Gallagher, S.E. Trask, C. Bauer, T. Woehrle, S.F. Lux, M. Tschech, P. Lamp, B. J. Polzin, S. Ha, B. Long, et al., Optimizing areal Capacities through understanding the limitations of lithium-ion electrodes, J. Electrochem. Soc. 163 (2016) A138–A149, https://doi.org/10.1149/2.0321602jes.
- [2] J. Janek, P. Adelhelm, Zukunftstechnologien, in: R. Korthauer (Ed.), Handbuch Lithium-Ionen-Batterien, Springer, Berlin, Heidelberg, 2013, pp. 199–217. ISBN 978-3-642-30653-2.
- [3] R. Koerver, W. Zhang, L. de Biasi, S. Schweidler, A.O. Kondrakov, S. Kolling, T. Brezesinski, P. Hartmann, W.G. Zeier, J. Janek, Chemo-mechanical expansion of lithium electrode materials – on the route to mechanically optimized all-solid-state batteries, Energy Environ. Sci. 11 (2018) 2142–2158, https://doi.org/10.1039/ C8EE00907D.
- [4] S.P. Culver, R. Koerver, T. Krauskopf, W.G. Zeier, Designing ionic conductors: the interplay between structural phenomena and interfaces in thiophosphate-based solid-state batteries, Chem. Mater. 30 (2018) 4179–4192, https://doi.org/ 10.1021/acs.chemmater.8b01293.
- [5] R. Koerver, I. Aygün, T. Leichtweiß, C. Dietrich, W. Zhang, J.O. Binder, P. Hartmann, W.G. Zeier, J. Janek, Capacity fade in solid-state batteries: interphase formation and chemomechanical processes in nickel-rich layered oxide cathodes and lithium thiophosphate solid electrolytes, Chem. Mater. 29 (2017) 5574–5582, https://doi.org/10.1021/acs.chemmater.7b00931.
- [6] J. Landesfeind, J. Hattendorff, A. Ehrl, W.A. Wall, H.A. Gasteiger, Tortuosity determination of battery electrodes and separators by impedance spectroscopy, J. Electrochem. Soc. 163 (2016) A1373–A1387, https://doi.org/10.1149/ 2.1141607ies.
- [7] J. Landesfeind, M. Ebner, A. Eldiven, V. Wood, H.A. Gasteiger, Tortuosity of battery electrodes: validation of impedance-derived values and critical comparison with 3D tomography, J. Electrochem. Soc. 165 (2018) A469–A476, https://doi. org/10.1149/2.0231803jes.
- [8] P. Minnmann, J. Schubert, S. Kremer, R. Rekers, S. Burkhardt, R. Ruess, A. Bielefeld, F.H. Richter, J. Janek, Editors' choice—visualizing the impact of the composite cathode microstructure and porosity on solid-state battery performance, J. Electrochem. Soc. 171 (2024) 060514, https://doi.org/10.1149/1945-7111/
- [9] Y. Fujii, A. Miura, N.C. Rosero-Navarro, Y. Mizuguchi, C. Moriyoshi, Y. Kuroiwa, M. Higuchi, K. Tadanaga, Reaction mechanism of FePS 3 electrodes in all-solid-state lithium secondary batteries using sulfide-based solid electrolytes, J. Electrochem. Soc. 165 (2018) A2948–A2954, https://doi.org/10.1149/2.0191813jes.
- [10] S.V. Patel, S. Banerjee, H. Liu, P. Wang, P.-H. Chien, X. Feng, J. Liu, S.P. Ong, Y.-Y. Hu, Tunable lithium-ion transport in mixed-halide argyrodites Li 6– x PS 5– x ClBr x: an unusual compositional space, Chem. Mater. 33 (2021) 1435–1443, https://doi.org/10.1021/acs.chemmater.0c04650.
- [11] A. Kato, M. Yamamoto, A. Sakuda, A. Hayashi, M. Tatsumisago, Mechanical properties of Li2S–P2S5 glasses with lithium halides and application in all-solidstate batteries, ACS Appl. Energy Mater. 1 (2018) 1002–1007, https://doi.org/ 10.1021/acsaem.7b00140.
- [12] M. Yamamoto, M. Takahashi, Y. Terauchi, Y. Kobayashi, S. Ikeda, A. Sakuda, Fabrication of composite positive electrode sheet with high active material content and effect of fabrication pressure for all-solid-state battery, J. Ceram. Soc. Jpn. 125 (2017) 391–395, https://doi.org/10.2109/jcersj2.16321.
- [13] M. Alabdali, F.M. Zanotto, M. Duquesnoy, A.-K. Hatz, D. Ma, J. Auvergniot, V. Viallet, V. Seznec, A.A. Franco, Three-dimensional physical modeling of the wet manufacturing process of solid-state battery electrodes, J. Power Sources 580 (2023) 233427, https://doi.org/10.1016/j.jpowsour.2023.233427.
- [14] A. Bielefeld, D.A. Weber, J. Janek, Modeling effective ionic conductivity and binder influence in composite cathodes for all-solid-state batteries, ACS Appl.

- Mater. Interfaces 12 (2020) 12821–12833, https://doi.org/10.1021/
- [15] P. Minnmann, L. Quillman, S. Burkhardt, F.H. Richter, J. Janek, Editors' choice—quantifying the impact of charge transport bottlenecks in composite cathodes of all-solid-state batteries, J. Electrochem. Soc. 168 (2021) 040537, https://doi.org/10.1149/1945-7111/abf8d7.
- [16] A. Bielefeld, D.A. Weber, J. Janek, Microstructural modeling of composite cathodes for all-solid-state batteries, J. Phys. Chem. C 123 (2019) 1626–1634, https://doi. org/10.1021/acs.jpcc.8b11043.
- [17] A. Bielefeld, D.A. Weber, R. Rueß, V. Glavas, J. Janek, Influence of lithium ion kinetics, particle morphology and voids on the electrochemical performance of composite cathodes for all-solid-state batteries, J. Electrochem. Soc. 169 (2022) 020539, https://doi.org/10.1149/1945-7111/ac50df.
- [18] A. Neumann, S. Randau, K. Becker-Steinberger, T. Danner, S. Hein, Z. Ning, J. Marrow, F.H. Richter, J. Janek, A. Latz, Analysis of interfacial effects in all-solidstate batteries with thiophosphate solid electrolytes, ACS Appl. Mater. Interfaces 12 (2020) 9277–9291, https://doi.org/10.1021/acsami.9b21404.
- [19] F. Strauss, T. Bartsch, L. De Biasi, A.-Y. Kim, J. Janek, P. Hartmann, T. Brezesinski, Impact of cathode material particle size on the capacity of bulk-type all-solid-state batteries, ACS Energy Lett. 3 (2018) 992–996, https://doi.org/10.1021/ acsenergylett.8b00275.
- [20] D. Hlushkou, A.E. Reising, N. Kaiser, S. Spannenberger, S. Schlabach, Y. Kato, B. Roling, U. Tallarek, The influence of void space on ion transport in a composite cathode for all-solid-state batteries, J. Power Sources 396 (2018) 363–370, https:// doi.org/10.1016/j.jpowsour.2018.06.041.
- [21] K.G. Naik, B.S. Vishnugopi, P.P. Mukherjee, Kinetics or transport: Whither goes the solid-state battery cathode? ACS Appl. Mater. Interfaces 14 (2022) 29754–29765, https://doi.org/10.1021/acsami.2c04962.
- [22] LAMMPS documentation (29 aug 2024 version) LAMMPS documentation, Available online: https://docs.lammps.org/Manual.html. (Accessed 30 September 2024).
- [23] M. Alabdali, F.M. Zanotto, B. Notredame, V. Viallet, V. Seznec, A.A. Franco, Experimental and computational analysis of slurry-based manufacturing of solidstate battery composite cathode, Batt. Supercaps (2024) e202400709, https://doi. org/10.1002/batt.202400709.
- [24] A.C. Ngandjong, T. Lombardo, E.N. Primo, M. Chouchane, A. Shodiev, O. Arcelus, A.A. Franco, Investigating electrode calendering and its impact on electrochemical performance by means of a new Discrete element method model: towards a digital twin of Li-ion battery manufacturing, J. Power Sources 485 (2021) 229320, https://doi.org/10.1016/j.jpowsour.2020.229320.
- [25] T. Lombardo, F. Lambert, R. Russo, F.M. Zanotto, C. Frayret, G. Toussaint, P. Stevens, M. Becuwe, A.A. Franco, Experimentally validated three-dimensional modeling of organic-based sodium-ion battery electrode manufacturing, Batt. Supercaps 5 (8) (2022) e202200116, https://doi.org/10.1002/batt.202200116.
- [26] S. Pinilla, F.M. Zanotto, D.Z. Dominguez, T. García, A.A. Franco, Carbon-binder-domain porosity extraction through lithium-ion battery electrode impedance data, Energy Storage Mater. (2024) 103818, https://doi.org/10.1016/j.ensm.2024.103818
- [27] M. Chouchane, A.A. Franco, An invitation to engage with computational modeling: user-friendly tool for in silico battery component generation and meshing, Batt. Supercaps 4 (9) (2021) 1451–1456, https://doi.org/10.1002/batt.202100096.
- [28] M. Chouchane, A. Rucci, A.A. Franco, A versatile and efficient voxelization-based meshing algorithm of multiple phases, ACS Omega 4 (2019) 11141–11144, https://doi.org/10.1021/acsomega.9b01279.

- [29] COMSOL documentation, Available online: https://doc.comsol.com/6.2/docserver/#!/com.comsol.help.comsol/helpdesk/helpdesk.html. (Accessed 30 September 2024).
- [30] Plateforme MatriCS Plateforme mutualisée pour les laboratoires de recherche de l'Université de Picardie Jules Verne.
- [31] R. Ruess, S. Schweidler, H. Hemmelmann, G. Conforto, A. Bielefeld, D.A. Weber, J. Sann, M.T. Elm, J. Janek, Influence of NCM particle cracking on kinetics of lithium-ion batteries with liquid or solid electrolyte, J. Electrochem. Soc. 167 (2020) 100532, https://doi.org/10.1149/1945-7111/ab9a2c.
- [32] M. Alabdali, F.M. Zanotto, M. Chouchane, A.C. Ngandjong, V. Viallet, V. Seznec, Y. S. Meng, A.A. Franco, Understanding mechanical stresses upon solid-state battery electrode cycling using Discrete element method, Energy Storage Mater. 70 (2024) 103527, https://doi.org/10.1016/j.ensm.2024.103527.
- [33] Casestudies for battery materials GeoDict simulation software, Available online: https://www.math2market.com/geodict-aplications/batteries.html. (Accessed 30 September 2024).
- [34] R. Amin, Y.-M. Chiang, Characterization of Electronic and Ionic Transport in Li 1-x Ni 0.33 Mn 0.33 Co 0.33 O 2 (NMC 333) and Li 1- x Ni 0.50 Mn 0.20 Co 0.30 O 2 (NMC 523) as a Function of Li Content, J. Electrochem. Soc. 163 (2016) A1512–A1517, https://doi.org/10.1149/2.0131608jes.
- [35] C. Liu, T. Lombardo, J. Xu, A.C. Ngandjong, A.A. Franco, An experimentally-validated 3D electrochemical model revealing electrode manufacturing parameters' effects on battery performance, Energy Storage Mater. 54 (2023) 156–163, https://doi.org/10.1016/j.ensm.2022.10.035.
- [36] B.L. Trembacki, A.N. Mistry, D.R. Noble, M.E. Ferraro, P.P. Mukherjee, S. A. Roberts, Editors' choice—mesoscale analysis of conductive binder domain morphology in lithium-ion battery electrodes, J. Electrochem. Soc. 165 (2018) E725–E736, https://doi.org/10.1149/2.0981813jes.
- [37] T. Lombardo, F. Lambert, R. Russo, F.M. Zanotto, C. Frayret, G. Toussaint, P. Stevens, M. Becuwe, A.A. Franco, Experimentally validated three-dimensional modeling of organic-based sodium-ion battery electrode manufacturing, Batter. Supercaps 5 (2022) e202200116, https://doi.org/10.1002/batt.202200116.
- [38] Naik, K.G.; Jangid, M.K.; Vishnugopi, B.S.; Dasgupta, N.P.; Mukherjee, P.P. Interrogating the role of stack pressure in transport-reaction interaction in the solid-state battery cathode. Adv. Energy Mater. n/a, 2403360, doi:10.1002/ aenm.202403360.
- [39] M. Chouchane, A. Rucci, T. Lombardo, A.C. Ngandjong, A.A. Franco, Lithium ion battery electrodes predicted from manufacturing simulations: assessing the impact of the carbon-binder spatial location on the electrochemical performance, J. Power Sources 444 (2019) 227285, https://doi.org/10.1016/j.jpowsour.2019.227285.
- [40] K.G. Naik, B.S. Vishnugopi, P.P. Mukherjee, Heterogeneities affect solid-state battery cathode Dynamics, Energy Storage Mater. 55 (2023) 312–321, https://doi. org/10.1016/j.ensm.2022.11.055.
- [41] T. Shi, Q. Tu, Y. Tian, Y. Xiao, L.J. Miara, O. Kononova, G. Ceder, High active material loading in all-solid-state battery electrode via particle size optimization, Adv. Energy Mater. 10 (2020) 1902881, https://doi.org/10.1002/ aenm.201902881.
- [42] E. Schlautmann, A. Weiß, O. Maus, L. Ketter, M. Rana, S. Puls, V. Nickel, C. Gabbey, C. Hartnig, A. Bielefeld, et al., Impact of the solid electrolyte particle size distribution in sulfide-based solid-state battery composites, Adv. Energy Mater. 13 (2023) 2302309, https://doi.org/10.1002/aenm.202302309.